[Article ID] 1003- 6326(2001)02- 0166- 07

Microstructural characteristics of intermetallic phases in spray-deposition Al-8.5Fe-1.3V-1.7Si alloy①

JIN Tou-nan(金头男)[1,2], XIAO Yu-de(肖于德)[1], LI Wen-xian(黎文献)[1],
YIN Zhi-min(尹志民)[1], LI Dou-xing(李斗星)[2]
(1. Department of Materials Science and Engineering, Central South University, Changsha 410083, P. R. China;
2. Laboratory of Atomic Imaging of Solids, Institute of Metals Research, Chinese Academy of Sciences, Shenyang 110015, P. R. China)

[Abstract] Analysis electron microtechnique (AEM) and high resolution electron microtechnique (HREM) studies were conducted on a spray deposition Al-8.5Fe-1.3V-1.7Si(mass fraction, %) alloy to determine the characteristics of the intermetallic phases. The results show that the striking characteristics of the microstructures in as-deposited and as-extruded alloys indicate the presence of a large amounts of homogeneously distributed fine particles and a few coarse particles, while small amount of eutectics consisted of α(Al) and α-AlFeSi are found in local zone in as-deposited alloy. The fine particle is identified to be bcc α-AlFeSi phase, and the coarse particles are monoclinic α-$Al_{13}Fe_4$ equilibrium phase, bcc α-AlFeSi phase and newly found hexagonal *h*-AlFeSi metastable phase. In α-$Al_{13}Fe_4$, stacking faults on (100) and (001) plane and microtwin on (100) twinning plane are frequently observed. The extra reflection spots in α-AlFeSi reflection pattern can be induced by α-AlFeSi superstructure. The hexagonal metastable phase transforms to bcc phase, and the compositions of two phases are very similar. A close crystallographic orientation relationship between hexagonal and bcc phases are determined, and HREM image shows that the interface between them is coherent.

[Key words] Al-Fe-V-Si alloy; spray casting, intermetallic phase, orientation relationship; phase interface
[CLC number] TG 132.3 [Document code] A

1 INTRODUCTION

Rapidly solidified (RS) Al-Fe-V-Si heat-resisting alloy has recently drawn much attention in astronavigation and aviation field for its excellent mechanical properties at both ambient and high temperatures, low density and low cost[1~3]. Previous studies showed that the main cause for maintaining enough strength and toughness of the alloy lies in the dispersive strengthening phase α-AlFeSi with low coarsening rate and high thermal stability. Therefore, most work concentrates on the formation of fine and homogeneous α-AlFeSi phase with large volume fraction and fine-grained matrix with supersaturated solute through RS technique, including casting, melt atomizing etc. Although the properties of the material prepared by spray deposition are not good enough due to low cooling rate, small amount and large-sized dispersoids, this method has potential in industry application for its simple process and high efficiency[4].

In order to obtain α-AlFeSi phase of large volume fraction, high contents of Fe, V and Si elements are added to form Al-Fe, Al-Fe-Si metastable and equilibrium phases with complex structure, for example, θ-$Al_{13}Fe_4$ equilibrium phase, micro-quasicrystal phase, icositetrahedron phase and newly found hexagonal metastable phase[5,6]. These phases will make the distribution of α-AlFeSi particles inhomogeneous, and worsen the stability of the material structure. This work aims at studying the structure characteristics and interface orientation of various phases in as-deposited and as-extruded Al-Fe-V-Si alloy by electronic microscopy, providing theoretical basis for the improvement of material properties.

2 EXPERIMENTAL

Firstly, Al-Fe, Al-Fe-V, Al-Si intermediate alloys were smelt in medium frequency induction furnace, then they were further smelt into a master alloy with nominal composition of Al-8.5Fe-1.3V-1.7Si (mass fraction, %) in an industry furnace. With self-made equipment, the alloy melt was atomized at 900 ℃ by nitrogen and deposited into a *d*250 mm cylinder. The cylinder was then hot extruded at 470 ℃ with an extrusion ratio of 16∶1. In order to study the solidification morphology of the melt, a 3 mm-thick sample was deposited and observed by JSM-6310F SEM at an accelerated voltage of 20 kV. Samples were cut from the as-deposited and as-extruded bar for TEM observation, and the foils were prepared by ion thinning. Electron diffraction

① [Foundation item] Project (G1999064900- 5) supported by the National Key Fundamental Research Development Program and project (95- YS - 010) supported by Key Program of the 9th Five-Year Plan of China [Received date] 2000- 03- 10; [Accepted date] 2000- 10- 11

(SAED) and high resolution image (HREM) were observed by JEOL-2010 electron microscope at an accelerated voltage of 200 kV; and X-ray energy spectrum analysis (EDAX) was finished on EDAX-9100 instrument at an accelerated voltage of 100 kV.

3 RESULTS AND DISCUSSION

3.1 Phase morphology and composition

The original morphologies of the atomized melt after depositing and solidification are shown in Fig. 1. Fig. 1(a) and Fig. 1(b) are the secondly electron (SE) images of the deposit face and lateral face respectively. The flake-like particles indicate that the melt solidifies after depositing. Fig. 1(c) and Fig. 1(d) show the TEM images of as-deposited sample. There are a large amount of fine spherical dispersoids (about 50 nm) and few coarse particles (Fig. 1(c)) homogeneously distributed, and in some area there appears eutectic microstructure (Fig. 1(d)).

In as-extruded alloy, its original eutectic microstructure is broken, but there is little variation in the morphology, size and distribution of coarse and fine dispersed particles, as shown in Fig. 1(c). By EDAX and SAED, it is found that most fine particles are bcc α-AlFeSi phases, the eutectic structure consists of α(Al) solid solution and α-AlFeSi phase, and the coarse particles can be divided into three types of phases, whose chemical compositions are listed in Table 1. Although there are V and Si elements in θ-$Al_{13}Fe_4$ phase, it still belongs to binary phase and V and Si are just dissolved in it. At the same time, there is V element dissolved in the two ternary phases. Usually V substitutes for Fe atom because they have similarity in atomic physical properties[7]. Table 1 also indicates that it is difficult to distinguish the three phases by EDAX because their compositions are almost the same.

Table 1 Chemical compositions of coarse particles by EDAX (%)

Phase	x(Al)	x(Fe)	x(V)	x(Si)
θ-$Al_{13}Fe_4$	76.13	22.27	0.42	1.18
α-AlFeSi	76.57	15.61	1.93	6.19
h-AlFeSi	76.36	15.91	1.84	5.87

3.2 Phase structure

3.2.1 θ-$Al_{13}Fe_4$ phase

θ-$Al_{13}Fe_4$ phase is a common equilibrium phase in Al-Fe base alloy with flake-like shape. Its structure was C2/m determined by X-ray diffraction primarily[8,9]. Fig. 2 shows [0$\bar{1}$0] and [001] electron diffraction patterns of θ-$Al_{13}Fe_4$ phases. Indexing

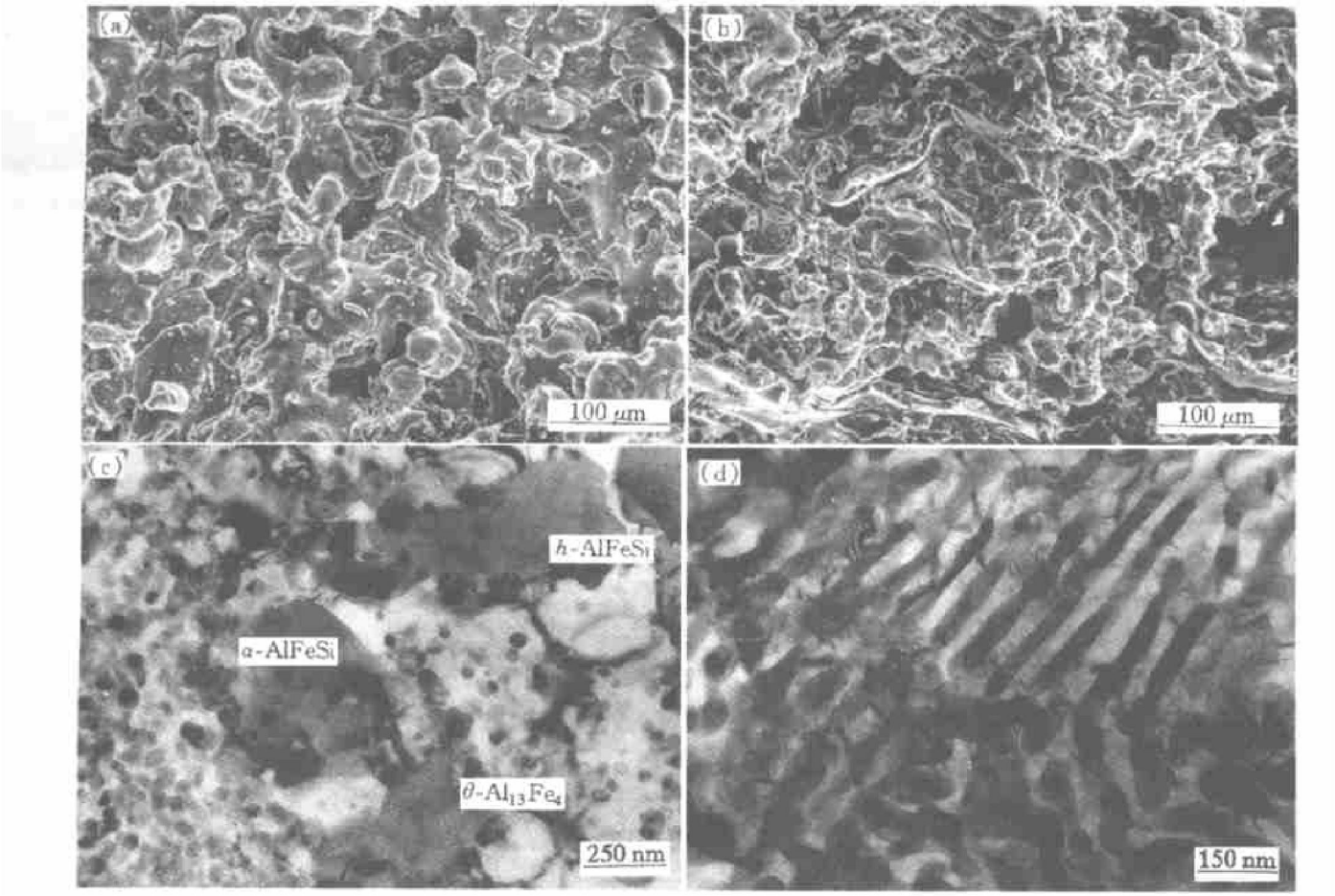

Fig. 1 SEM micrographs of deposit in horizontal section (a) and vertical section (b), TEM images of intermetallic phases (c) and fine eutectic phases (d) of as-deposited sample

results show that the diffraction forbidden condition of $h+k=2n+1$ is satisfied and the monoclinic angle can be directly obtained from Fig. 2(a) (its lattice structural parameters are listed in Table 2), which coincide with that of X-ray diffraction pattern.

Table 2 Crystal structure of intermetallic phases

Phase	Bravais lattice	Lattice parameters	Space group
θ-$Al_{13}Fe$	C-centered monoclinic	$a=1.549$ nm $b=0.808$ nm $c=1.248$ nm $\beta=107.75°$	C2/m
α-AlFeSi	Body-centered cubic	$a=1.256$ nm	Im3
α-AlFeSi superstructure	Rhombohedral	$a=3.076$ nm $c=3.26$ nm	$R\bar{3}$
α_T-AlFeSi	C-centered monoclinic	$a=2.795$ nm $b=3.062$ nm $c=2.073$ nm $\beta=97.74°$	C2/m
h-AlFeSi	Hexagonal	$a=2.514$ nm $c=1.257$ nm	P6/mmm

Another apparent characteristic of θ-$Al_{13}Fe_4$ phase is high content of twins and stacking faults. From Fig. 2(a), it can be deduced that the twinning face is (100) plane. The line patterns induced by faults and micro-twins are parallel to $[200]^*$ and $[001]^*$ reciprocal vector, which means that the faults and micro-twinning face may be two types: (100) and (001). Fig. 3 shows the crystal lattice of θ-$Al_{13}Fe_4$ phase along [010] direction. There are a large number of faults and microtwins, dividing the crystal into small domains of several to tens nanometer. The displacement of every two domains is about half the lattice distance, indicating that the fault vector is $a/2[100]$ or $c/2[001]$.

3.2.2 α-AlFeSi phase

Cubic α-AlFeSi phase is the main strengthening phase in Al-Fe-V-Si heat-resisting alloy. Most phase is near spherical with size of 50 nm dispersing in the alloy, while some irregular coarse α-AlFeSi particles also exist (as shown in Fig. 1(c)). Fig. 4 is the electron diffraction pattern of α-AlFeSi phase. According to the crystal structure reported by Cooper[10, 11], α-AlFeSi phase has two types of space lattice: primary cubic Pm3 and bcc Im3. By indexing, the diffraction patterns in Fig. 4 belong to bcc structure. No simple cubic α-AlFeSi phase was detected in this work.

By the intensity distribution of the diffraction spots in the [111] direction, α-AlFeSi phase shows 3-fold rotation symmetry (Fig. 4(c)), but in the [001] direction only 2-fold rotation axis and mirror symmetry exist and no 4-fold rotation symmetry exists (Fig. 4(a)). Distribution of diffraction intensity also shows that the intensity of all the (*hkl*) diffraction in the same (*hkl*) crystal group is not equal, e.g. (530) and (350), $(5\bar{3}2)$ and $(5\bar{2}3)$. Detailed observation shows that the (*hkl*) index can only exchange cyclically, not randomly. The above diffraction characteristics are correlated to Im3 space group of low symmetry. Fig. 4 also indicates that the diffraction of some {530}, {532} and {600} is very strong, which is related to the crystal structure of α-AlFeSi phase. According to the bond energy calculation of empirical electron theory[12], ⟨530⟩, ⟨532⟩ and ⟨600⟩ are strong bonding orientations in α-AlFeSi phase, hence the lattice face perpendicular to these orientations shows strong diffraction.

3.2.3 α-AlFeSi phase superstructure

As shown in Fig. 5, some bcc α-AlFeSi particles exhibit extra spots. Dons[13] thought that these extra diffraction spots are induced by α_T-AlFeSi phase, which has a C-centered monoclinic structure and the

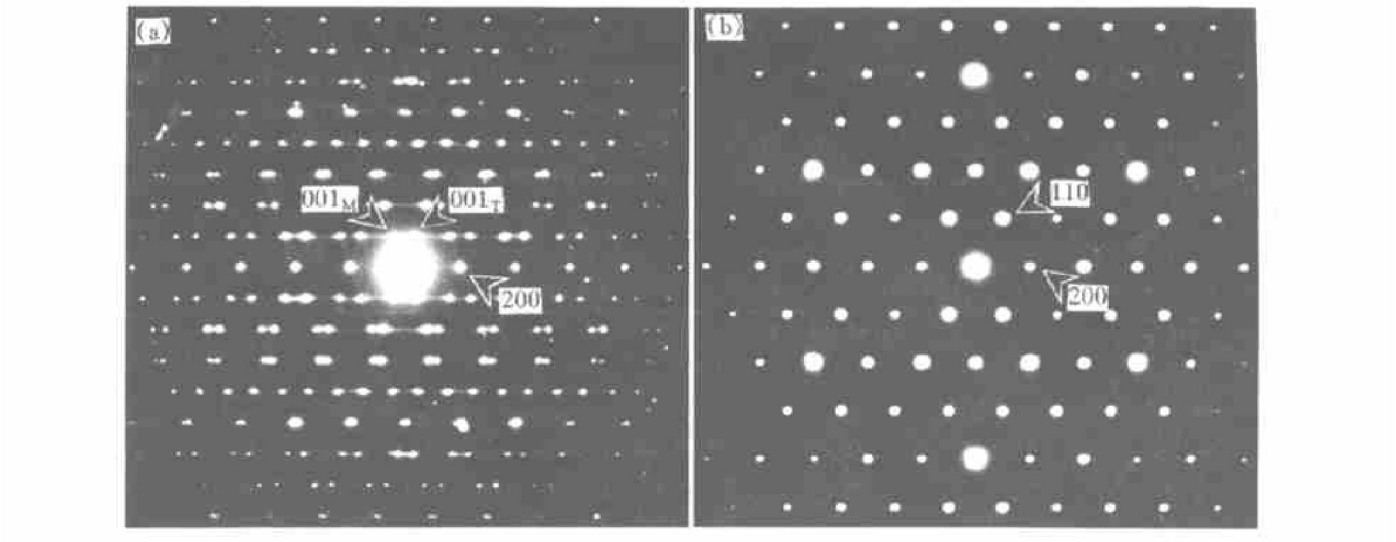

Fig. 2 SAED patterns of θ-$Al_{13}Fe_4$ phase along different zone axes
(a) —$[0\bar{1}0]$; (b) —[001]

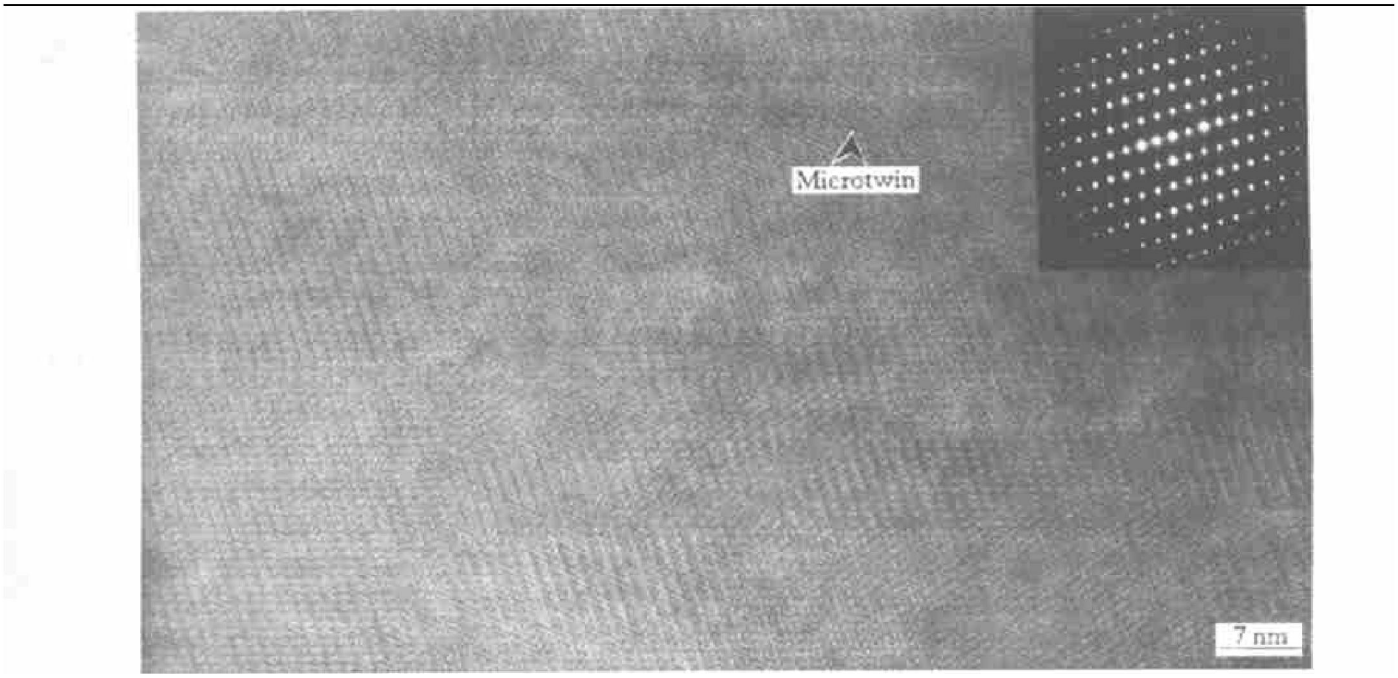

Fig. 3 HREM images of θ-$Al_{13}Fe_4$ phase in [010] orientation

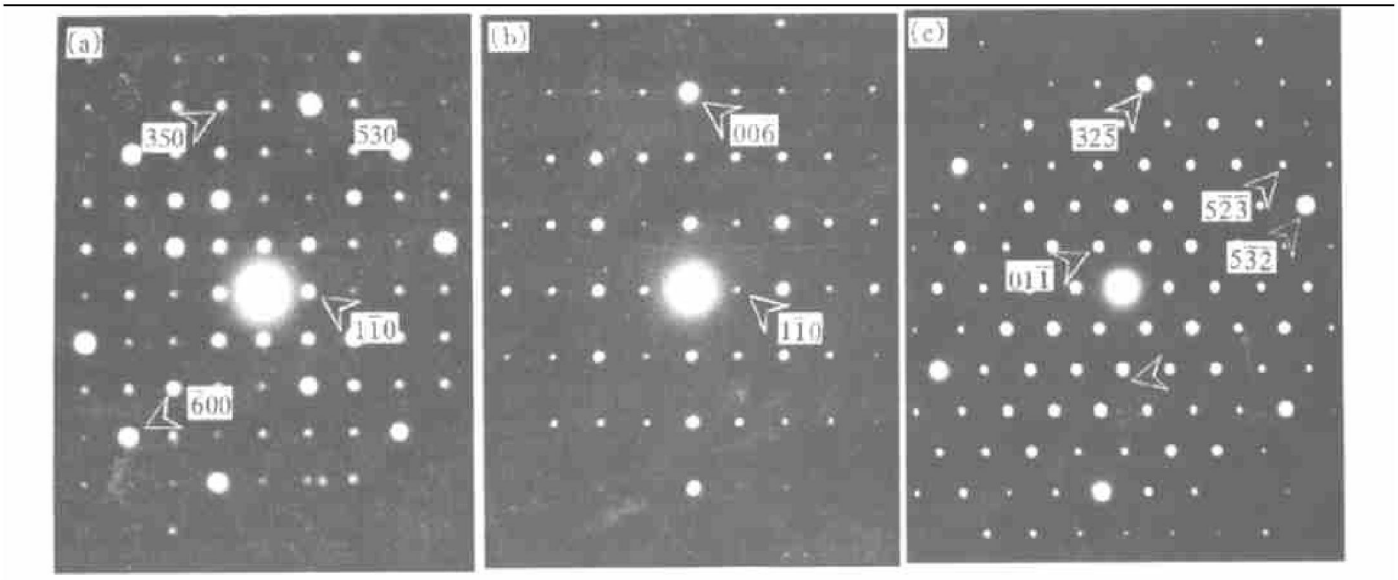

Fig. 4 SAED patterns of α-AlFeSi phase along different zone axes
(a) —[001]; (b) —[110]; (c) —[111]

three basic axes are $a = [120]_{bcc}$, $b = [\bar{2}11]_{bcc}$ and $c = 1/2[1\bar{1}3]_{bcc}$ (as listed in Table 2). Liu et al[14] studied the extra diffraction of α-AlFeSi phase by convergent beam electron diffraction and EDAX, and found that an α-AlFeSi superstructure phase forms with a space group of $R\bar{3}$, in which the ordered Fe atom vacancy in the bcc α-AlFeSi makes the movement cycle of bcc lattice along $\langle 111\rangle_{bcc}$ and $\langle 112\rangle_{bcc}$ direction increase by three times. Both the above two structure models can be used to index the extra diffraction spots in Figs. 5(d) ~ (g) coincidentally by itself, but they have shortcomings. The diffraction patterns of some axes are not coincidental by the former model[14], and no three-time $(111)_{bcc}$ and $(112)_{bcc}$ face arrangement cycles were observed in α-AlFeSi crystal lattice expected by the later model. Fig. 5(c) shows the diffraction pattern with two variations of the superstructure.

3.2.4 *h*-AlFeSi metastable phase

Hexagonal metastable phase was newly found by Koh et al[6] in RS Al-Fe-V-Si alloy, and its formation was related to the undercooling of the melt. Its space group is P6/mmm, and lattice parameters are a = 2.514 nm and c = 1.257 nm, but its composition, atomic type and distribution were not determined yet. This metastable phase was also observed in this work. Fig. 6 shows its electron diffraction pattern, which is perfectly coincidental to the structure parameters reported by Koh. EDAX results in Table 1 show that the composition of the hexagonal phase is very close

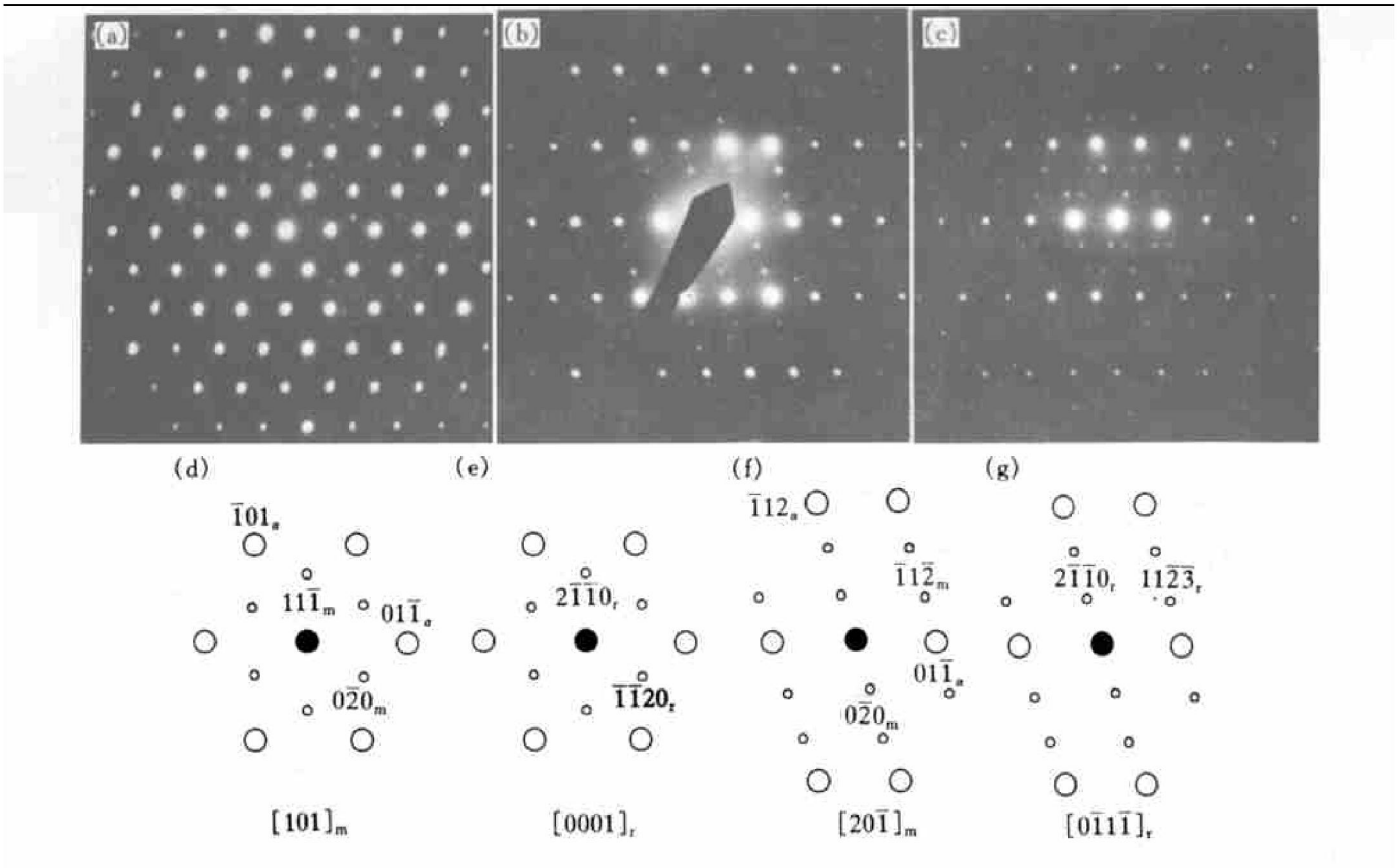

Fig. 5 SAED patterns with extra reflections in bcc α-AlFeSi phase
(a) —$[111]_{bcc}$; (b) —$[311]_\alpha$; (c) —Extra reflections from two variants of superlattice phase; (d) and (f) —Schematic diagrams of monoclinic lattice; (e) and (g) —Schematic diagrams of rhombohedral superlattice

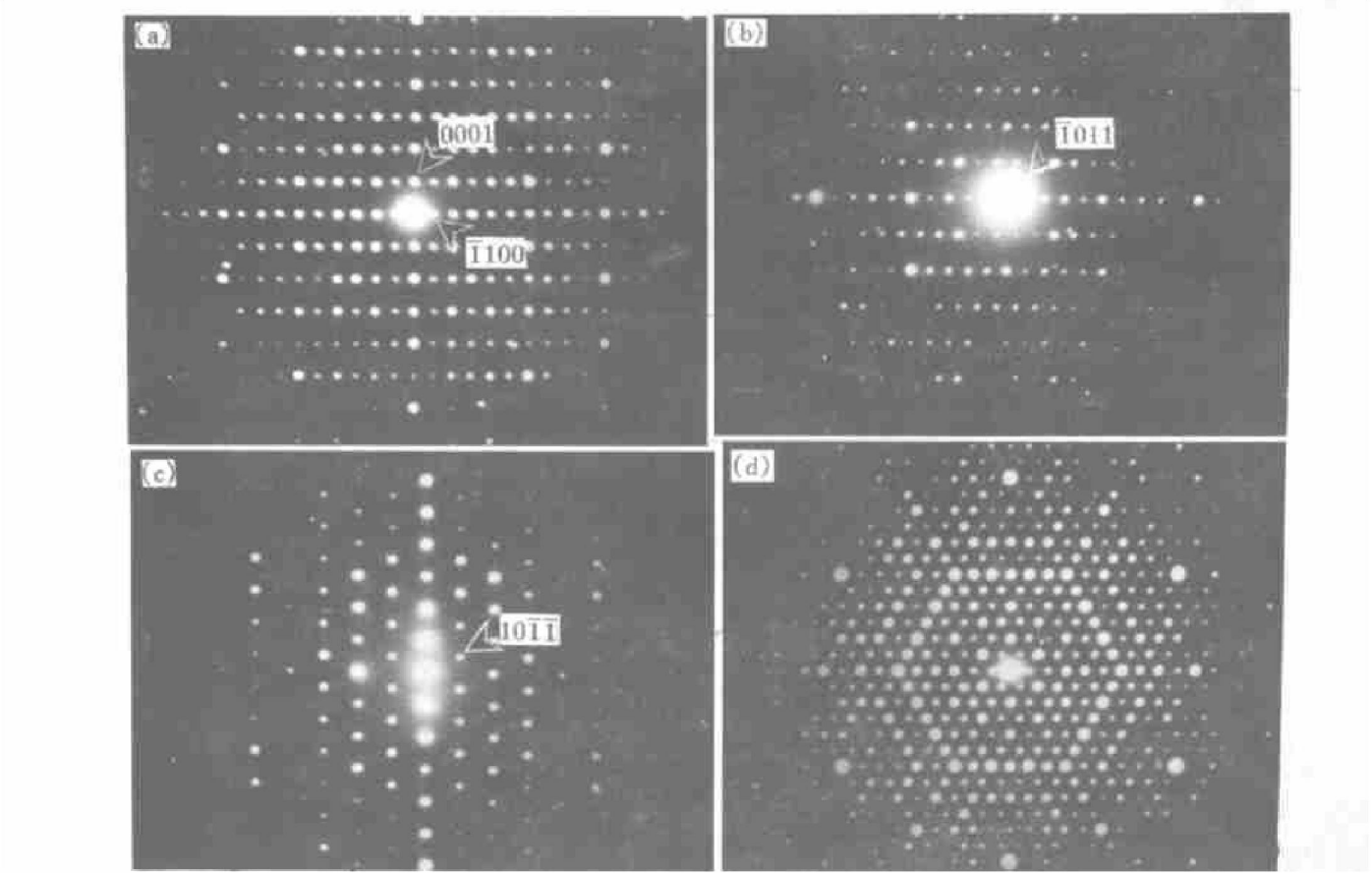

Fig. 6 SAED patterns of *h*-AlFeSi hexagonal phase along different zone axes
(a) —$[11\bar{2}0]$; (b) —$[11\bar{2}3]$; (c) —$[01\bar{1}1]$; (d) —[0001]

to that of bcc α-AlFeSi, so it is called as *h*-AlFeSi phase in this paper. By close observation, the transformation of *h*-AlFeSi to bcc α-AlFeSi can be found in Fig. 7, proving that this phase is metastable. The above results indicate that there is a structural relationship between the phase structure of *h*-AlFeSi and bcc AlFeSi. By comparing Fig. 4(c) and Fig. 6(d), it can be found that the strong diffraction spots of the two phases are coincidental, hence their structure units are probably the same. Therefore, it is possible to deduce the crystal structure of *h*-AlFeSi by comparing the HERM of the specific orientation of the two phases and simulating the hexagonal structure using the structure unit of α-AlFeSi.

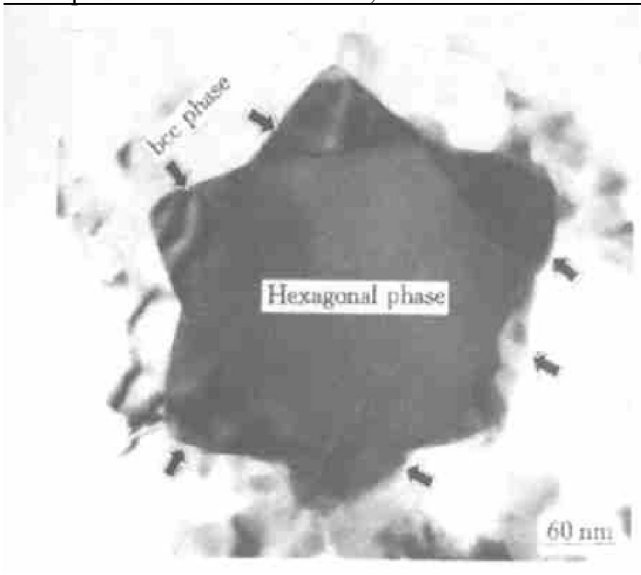

Fig. 7 Adjacent hexagonal and bcc phases

3.3 Orientation relationship between α-AlFeSi and *h*-AlFeSi phases

Fig. 7 shows the transformation of *h*-AlFeSi to bcc α-AlFeSi. It can be seen that bcc phase grows preferentially on the six prismatic faces of the hexagonal phase. Fig. 8 shows the composite diffraction and its illustration. By determination, these diffraction patterns indicate the same orientation relationship. The index transformation matrix of parallel relationship is

$$\begin{bmatrix} u \\ v \\ w \end{bmatrix} = \boldsymbol{N}\begin{bmatrix} U \\ V \\ W \end{bmatrix}, \quad \begin{bmatrix} h \\ k \\ l \end{bmatrix} = \boldsymbol{N}^{\mathrm{T}}\begin{bmatrix} U \\ V \\ W \end{bmatrix} \tag{1}$$

$$\boldsymbol{N} = \begin{bmatrix} 1 & 1 & 0 \\ 1.73 & -1.73 & 0 \\ 0 & 0 & 1 \end{bmatrix}$$

The orientation relationship between two phases is: $(001)_{bcc} \parallel (0001)_{hex}$, $[010]_{bcc} \parallel [1\bar{1}00]_{hex}$, $[100]_{bcc} \parallel [11\bar{2}0]_{hex}$

Fig. 9 is the HREM of the phase interface of *h*-AlFeSi and bcc phases, the electron beam is along

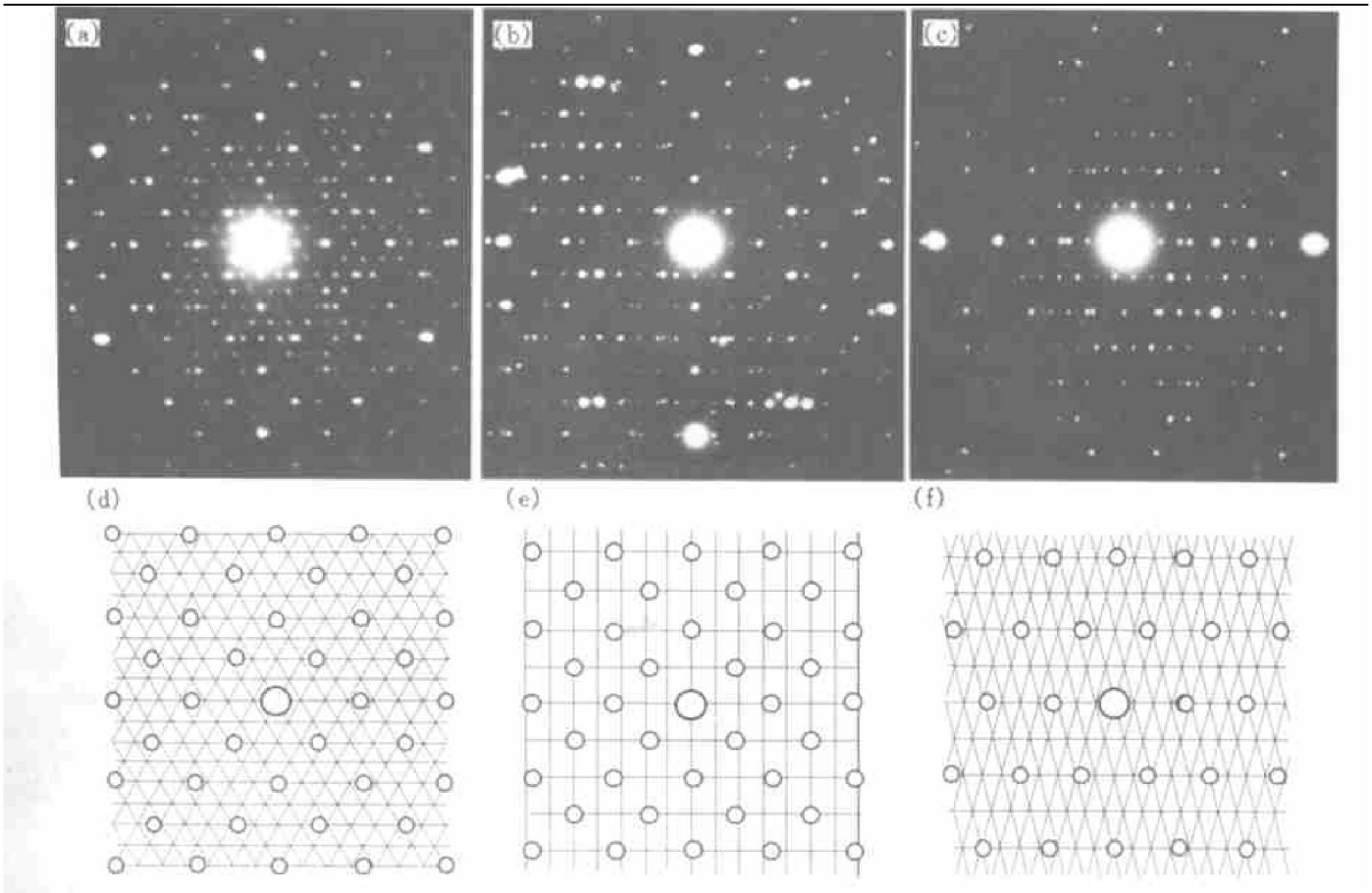

Fig. 8 Composite SAED patterns of bcc and hexagonal phases with their schematic diagram
(a) and (d) —$[0001]_{hex} \parallel [001]_{bcc}$; (b) and (e) —$[11\bar{2}0]_{hex} \parallel [100]_{bcc}$; (c) and (f) —$[11\bar{2}3]_{hex} \parallel [201]_{bcc}$

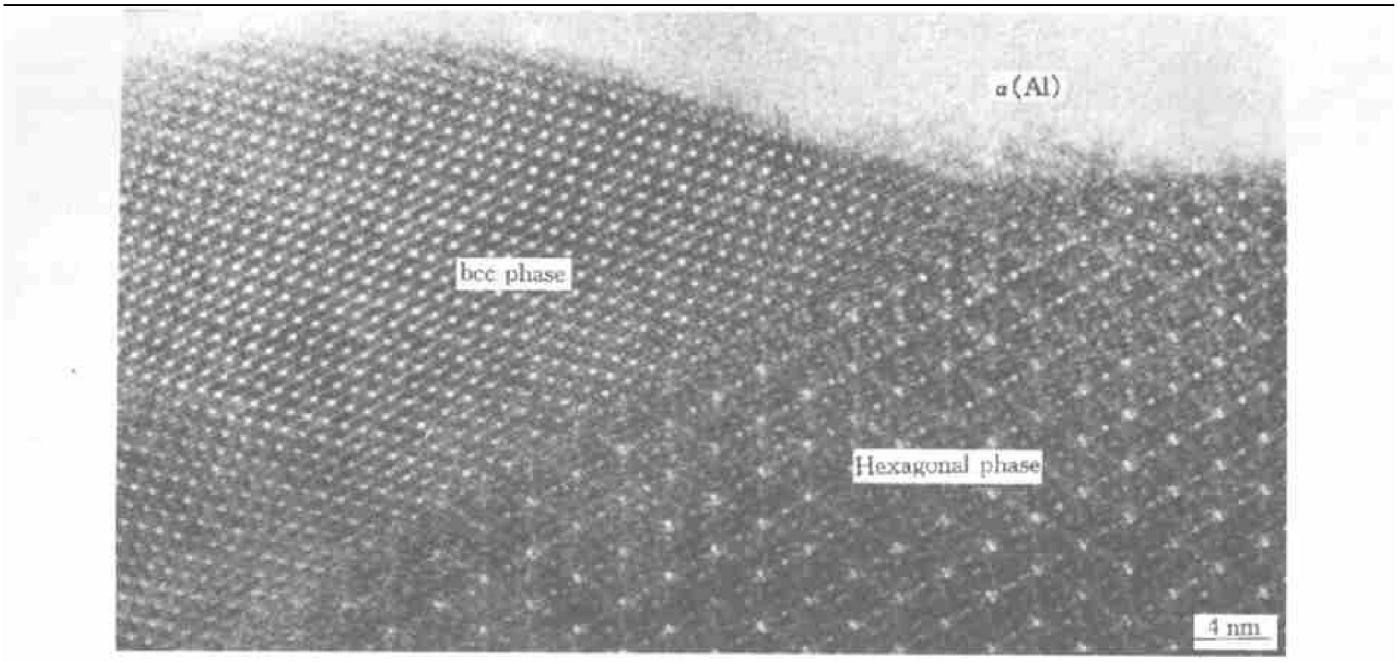

Fig. 9 HREM image of interface of hexagonal and bcc phases in $[0001]_{hex}$ or $[001]_{bcc}$ orientation

$[001]_{bcc}$ and $[0001]_{hex}$ direction. It can be seen that the phase interface belongs to $(010)_{bcc}$ of bcc phase or $(1\bar{1}00)_{hex}$ of hexagonal phase, and in the interface, $[11\bar{2}0]_{hex} = 2[100]_{bcc}$, indicating that the interface between α-AlFeSi and *h*-AlFeSi phase is perfectly coherent.

4 CONCLUSIONS

1) There are a large amount of bcc α-AlFeSi dispersoids with size of 50 nm and small coarse particles in the as-deposited Al-8.5Fe-1.3V-1.7Si heat-resisting alloy. After the subsequent hot working, the size of the dispersoids has not changed. The coarse particles include θ-$Al_{13}Fe_4$ equilibrium phase, hexagonal *h*-AlFeSi metastable phase and α-AlFeSi phase.

2) There are a large number of stacking faults and microtwins in θ-$Al_{13}Fe_4$ phase, and some α-AlFeSi particles show superstructure.

3) The hexagonal *h*-AlFeSi metastable phase transforms to bcc α-AlFeSi phase, and their chemical compositions are almost the same.

4) There is strict orientation relationship between hexagonal *h*-AlFeSi metastable phase and bcc α-AlFeSi phase: $(001)_{bcc} \parallel 0001_{hex}$, $[010]_{bcc} \parallel [1\bar{1}00]_{hex}$, $[100]_{bcc} \parallel [11\bar{2}0]_{hex}$, and their phase interface is coherent.

[REFERENCES]

[1] Skinner D J, Bye R L and Rayhoud D. Dispersion strengthened Al-Fe-V-Si alloy [J]. Scripta Metall, 1986, 20: 867- 872.

[2] Frank R E and Hawk J A. Effect of very high temperatures on the mechanical properties of AlFeVSi alloy [J]. Scripta Metall, 1989, 23: 113- 115.

[3] Chellman D J, Ekvall J C and Rainen R A. Elevated temperature PM aluminum alloy for aircraft structure [J]. Metall Powder Rep, 1988, 43: 672- 675.

[4] CHEN Zheng-hua, JIANG Xiang-yang, WANG win, et al. Formation characteristics of Al-Cu-Fe-Mg, Al-Cu-Fe-Zn and Al-Cu-Fe-Zn-Mg quasicrystals [J]. J Cent South Inst Min Metal, (in Chinese), 1992, 23(3): 328- 334.

[5] Skjerpe P. Intermetallic phases formed during DC-casting of an Al-0.25wt pct Fe-0.13 wt pct Si alloy [J]. Metall Trans, 1987, 18A: 189- 200.

[6] Koh H J, Park W J and Kim N J. Identification of metastable phases in strip-cast and spray-cast Al-Fe-V-Si alloys [J]. Mat Trans JIM, 1998, 39: 982- 988.

[7] Rodriguez M A and Skinner D J. Compositional analysis of the cubic silicide intermetallic in dispersion strengthened Al-Fe-V-Si alloys [J]. J Mater Sci Lett, 1990, 9: 1292- 1293.

[8] Black P J. The structure of $FeAl_3$ I [J]. Acta Cryst, 1955, 8: 43- 48.

[9] Black P J. The structure of $FeAl_3$ II [J]. Acta Cryst, 1955, 8: 175- 181.

[10] Cooper M and Robinson K. The crystal structure of the ternary alloy α(AlMnSi) [J]. Acta Cryst, 1966, 20: 614- 617.

[11] Cooper M. The crystal structure of the ternary alloy α(AlFeSi) [J]. Acta Cryst, 1967, 23: 1106- 1107.

[12] WANG J Q, QIAN C F, ZHANG B J, et al. Valence electron structure analysis of the cubic silicide intermetallics in rapidly solidified Al-Fe-V-Si alloy [J]. Scr Metall Mater, 1996, 34: 1509- 1514.

[13] Dons A L. Formation of intermetallic compounds during DC casting of a commercial purity Al-Fe-Si alloy [J]. Z Metallkde, 1985, 76: 151- 153.

[14] Liu P and Dunlop G L. Long range ordering of vacancies in bcc α-AlFeSi [J]. J Mater Sci, 1988, 23: 1419 - 1423.

(Edited by YANG Bing)